EARTHQUAKE RESPONSE AND DAMAGE PREDICTION OF REINFORCED CONCRETE MASONRY MULTISTORY BUILDINGS PART II: SELECTED RESULTS

by

G. A. Hegemier[I], W. Nachbar[II], G. Krishnamoorthy[III], B. Barclay[IV]

SYNOPSIS

Sample results from the research program outlined in Part I are presented in this paper.

INTRODUCTION

An extensive research effort on concrete masonry was outlined in Part I. It is the purpose of this paper to present sample results obtained to-date under this program. The discussion is confined to basic features of experimental data and analysis. Design recommendations are not made herein; the latter must await completion of appropriate test series, comprehensive data reduction, and interpretation. The results prescribed below were obtained from specimens constructed from the following constituents: 8 x 8 x 16-inch Type N normal weight concrete block (ASTM C90), Type S mortar (ASTM C270), and 2000 psi fine grout (ASTM C476).

DISCUSSION OF BIAXIAL TESTS

A complete description of the biaxial tests is beyond the scope of this presentation. For simplicity, attention is focused below upon the failure surface for fully grouted but unreinforced specimens. This represents the first step in understanding the macro-behavior of concrete masonry and hence is worthy of discussion. The intersection of the failure surface with the plane $N_{11}' = 0$ (see Part I) is illustrated in Figs. 1a, b. This represents the case where the normal stress on head-joint planes vanishes or is small in relation to the normal and shear stresses on bed-joint planes. The rays in Figs. 1a, b represent the

---

I Professor, Dept. Appl. Mechs. & Engg. Sci., University of California, San Diego, La Jolla, CA.
II Professor, Dept. Appl. Mechs. & Engg. Sci., University of California, San Diego, La Jolla, CA.
III Professor, Dept. Civil Engg., San Diego State University, San Diego.
IV Principal Engineer, Agbabian Associates.

layup angles and the corresponding proportional loading described in Part I. Data points, which represent statistical means of repeated tests, are denoted by circles. Stresses shown are based upon net cross-sectional areas.

Two basic failure modes were observed in these tests. In the tension zone, and in the compression zone for $\theta > 20^\circ$, a brittle joint-failure was observed as illustrated in Fig. 5 ($\theta = 45^\circ$). In the compression zone for $\theta < 20^\circ$ failure consisted of multiple cracks through joints, face-shells, and grout; a degree of energy absorption was also observed. This mode of failure is illustrated in Fig. 4 for $\theta = 15^\circ$.

The curves in Figs. 1a, b represent several macroscopic, analytical failure models considered to-date. The dashed curve is based upon the premise that failure occurs when a principal stress reaches either the tensile strength or the compressive strength associated with a uniaxial, 0°-layup test. The solid curves result from the premise that the failure envelope in principal stress-space is piece-wise linear in the tension-compression and tension-tension zones as illustrated in Fig. 2 for concrete under biaxial stress states. [The two solid curves in Figs. 1a, b correspond to different estimated (from prism tests) compressive strengths, but the same (measured) 0°-layup uniaxial strength.] This model is seen to provide a more accurate description of material behavior. It is expected that the inclusion of anisotropic effects will further improve analytical-experimental correlation.

Finite element simulations of panel behavior have been performed to assess the accuracy of current micro-modeling concepts. The panel assembly is discretized into a system of plane stress finite elements. The grouted block and the adjacent mortar are represented by a single material whose properties are determined by a volume-based mixture procedure. The masonry joints are represented by an interface utilizing the interface implementation technique discussed in reference [3] of Part I. Interface properties are determined from the joint tests discussed in the following section. A typical fracture pattern for a 45° uniaxial case is shown in Fig. 3; this discretized system has 1674 degrees-of-freedom and a bandwidth of 154. The results of analysis performed to-date, which were obtained by using an out-of-core version of NONSAP, show excellent correlation with experimental data; for example, the ultimate strength of the model shown in Fig. 3 was about 77 psi, compared to 80 psi obtained experimentally.

DISCUSSION OF SMALL-SCALE TESTS

Joint Behavior — Data on joint fracture and post-fracture behavior is a prerequisite to a basic understanding of failure processes, and is a

necessary step in modeling on the macro-scale. A typical test-setup for monotonic loading of full-blocks is illustrated schematically in Fig. 6. In each test a constant normal stress was maintained across joint-planes, and the shear-stress distribution on these planes was varied by driving the center block in displacement control. Figures 6 - 9 exemplify typical static and dynamic behavior for grouted and ungrouted bed joints. The following basic characteristics are noted: 1) joint fracture-strength increases monotonically with precompression up to a block-failure transition; 2) under precompression exceeding 100 psi, post-fracture load decreases with displacement (Fig. 6) in a relatively smooth manner to a limiting value which, in turn, depends upon the level of precompression; 3) no discernible rate-dependence is evident in the ranges .01 to .50 in/sec under monotonic loading (Fig. 7) and in the range .05 to .50 Hz under cyclic loading; 4) cyclic experiments (Fig. 8) indicate that, following the first load reversal, load-displacement history is a function only of total displacement-path length and is not direction-sensitive; 5) ultimate strength of head joints, and ungrouted bed joints is considerably less than associated grouted bed joints; 6) in the absence of precompression, joint behavior is brittle—ungrouted bed and head joints exhibit extremely low (3 - 30 psi) shear and tensile strengths as well as large data-scatter.

Joint shear force V vs. displacement δ data suggested that the post-fracture regime could be represented by solutions of the differential equation

$$dV(\delta)/d\delta = -c[V(\delta) - V_\infty] , \qquad (1)$$

where V_∞ denotes the asymptote at "infinite" displacement and c is a function of the work $W(\delta)$ done up to the displacement δ, viz.,

$$W(\delta) = \int_{\delta_1}^{\delta} V(\delta')\, d\delta' . \qquad (2)$$

Using the following solution of (1),

$$[V(\delta) - V_\infty]/[V_1 - V_\infty] = \exp\left[-\left\{\bar{c}\int_{\delta_1}^{\delta} [W(\delta')]^{1/3}\, d\delta' + b\right\}\right] , \qquad (3)$$

where δ_1 corresponds to the maximum shear force V_1, a nonlinear regression method was developed to determine the constants $\bar{c}$, b, and V_∞ and the correlation shown in Fig. 6 was obtained. The points denote statistical means from at least three tests. Agreement is remarkable.

Finite element simulation of the joint tests was performed as a first step in the micro-modeling process. Local properties were established which enabled the analysis to match experimental V vs. δ data and which are reasonable when judged against independent measurements of

interface strength. A typical correlation for ungrouted bed joints is shown in Fig. 9. Agreement is seen to be good. Details of this work are contained in reference [3] of Part I. Subsequent to "tuning" the simulation on joint data, the above finite element model was utilized to predict biaxial panel behavior without further "tuning."

Prisms—Present working stress and design methods are based primarily upon a knowledge of the masonry compressive strength, f'_m. In practice f'_m is usually determined by prism tests. Current masonry codes and design recommendations (reference [1] of Part I) either explicitly or implicitly recommend that f'_m be computed on the basis of 2-course prisms laid in stacked bond, and capped according to ASTM C140 wherein a sulphur fly-ash compound or a high-strength gypsum plaster is used. Test procedures correspond to ASTM E447. Code correction factors purport to enable conversion of the strength of a particular geometry to that of a standard prism. A correction factor of unity is presently applied to the 2-course prism ($h/d = 2.0$). This evidently implies that a strong correlation with $h/d = 2.0$ and full-scale masonry exists. Our research clearly indicates this premise to be false and nonconservative. In particular, test data indicates that prism strength is significantly influenced by load-platen restraint and, in the absence of a soft capping material, is a strong function of the number of courses. A typical example is illustrated in Fig. 10. The data was obtained from full-block, fully-grouted specimens; precision-cutting to the desired h/d ratio was utilized in place of a high-strength capping material. The bearing platens at each end consisted of solid 8 X 8 X 16-inch aluminum blocks. Platen restraint resulted in a shear-mode failure in 2-course prisms, and a combined shear-tensile splitting in 3-course prisms. Proper tensile splitting was observed in 4- and 5-course prisms. Based upon the 5-course data, the 2-course results are 50 percent too high. Also, the data indicates that prism strength is a function of the number of joints in the specimen as well as the h/d ratio. Finally, an extensive literature review (reference [1], Part I) revealed an amazing fact: Virtually all code correction factors for prisms geometry are based upon a common source—the preliminary and exploratory investigation by Krefeld (see reference [2], Part I) on brick. This is patently unjustified.

CONCLUSIONS

1) Excellent correlation has been obtained to-date between experimental results and finite element modeling on the micro-scale. In particular, it appears that the macro-behavior of concrete masonry can be rationally predicted from masonry constituent properties.

2) Small-scale tests (e. g., prisms) raise some serious questions concerning the present method of determining masonry strength.

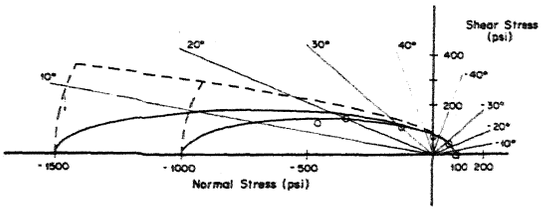

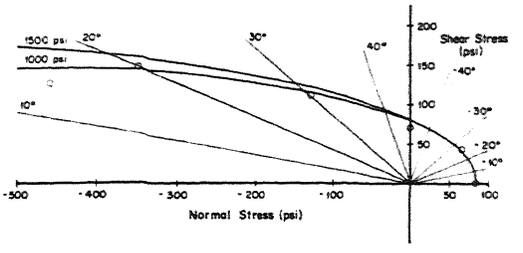

Figs. 1 a, b Failure envelopes.

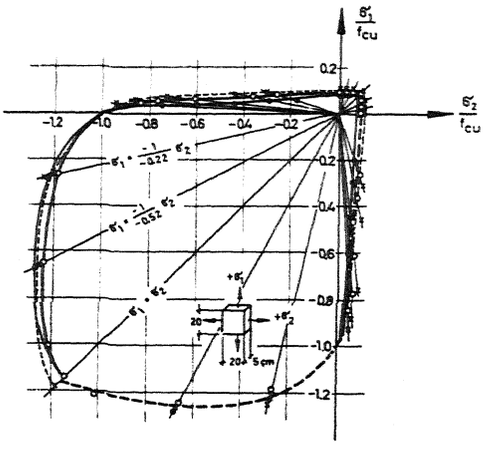

Fig. 2 Biaxial strength of concrete.

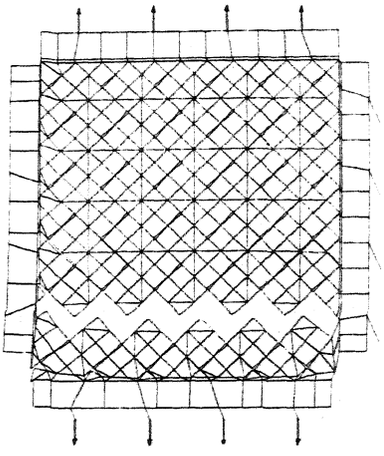

Fig. 3 Finite element prediction of failure.

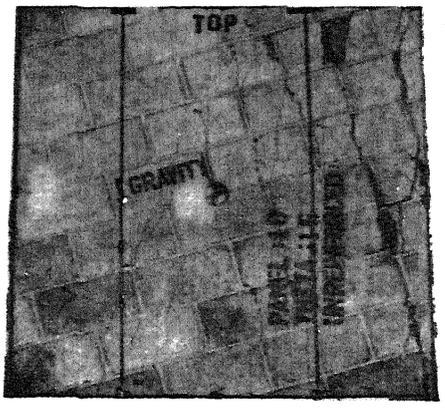

Fig. 4 Typical material failure.

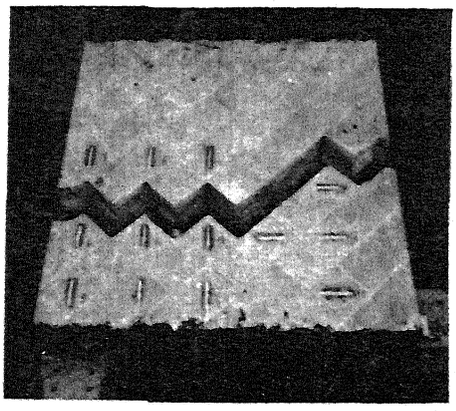

Fig. 5 Typical joint failure.

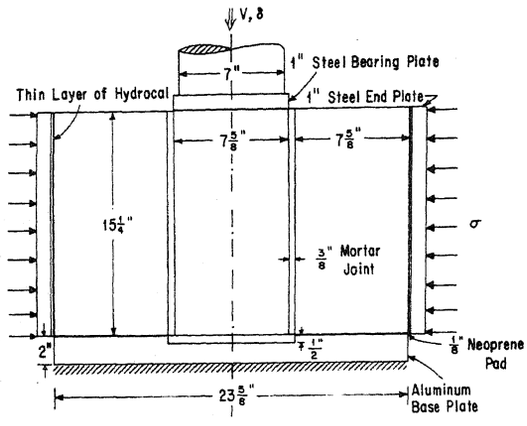

Fig. 5 Joint Test Setup.

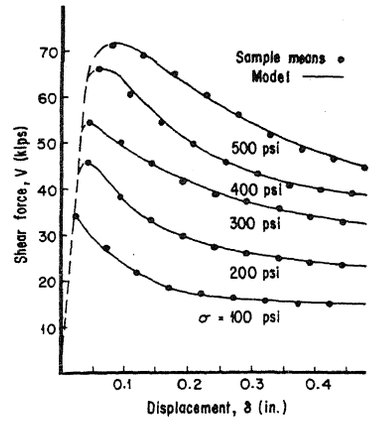

Fig. 6 Behavior of Bed Joints Under Precompression.

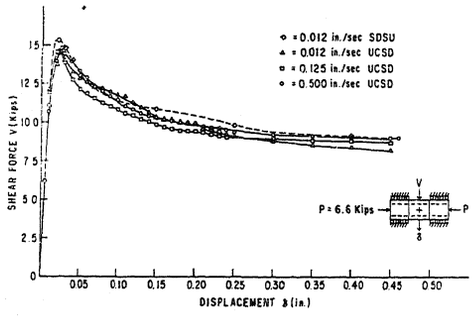

Fig. 7 Strain-Rate Dependence.

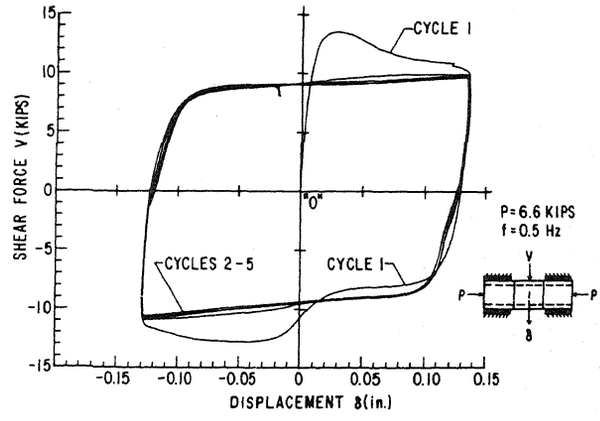

Fig. 8 Joint Behavior Under Cyclic Loading.

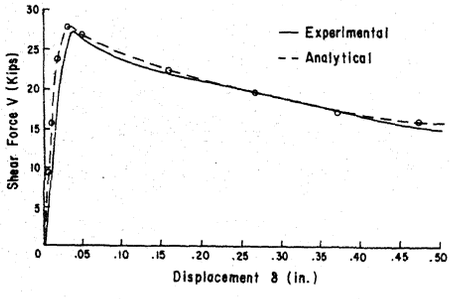

Fig. 9 Finite Element Simulation of Joint Behavior.

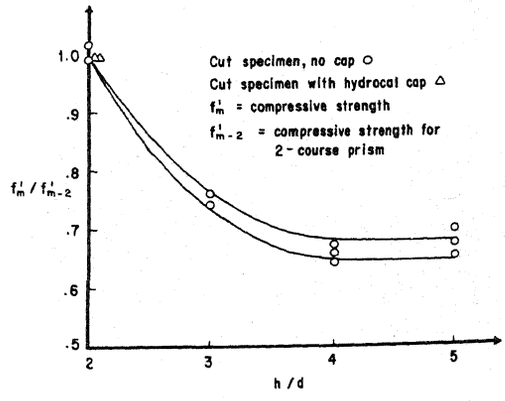

Fig. 10 Correlation of Prism Strength and Geometry.